FINAL REPORT

Demonstration of Advanced EMI Models for Live-Site UXO Discrimination at San Luis Obispo, California

SERDP Project MR-1572

SERDP
DOD ∙ EPA ∙ DOE

1. REPORT DATE **AUG 2012**	2. REPORT TYPE	3. DATES COVERED **00-00-2012 to 00-00-2012**

4. TITLE AND SUBTITLE **Demonstration of Advanced EMI Models for Live-Site UXO Discrimination at San Luis Obispo, California**	5a. CONTRACT NUMBER
	5b. GRANT NUMBER
	5c. PROGRAM ELEMENT NUMBER
6. AUTHOR(S)	5d. PROJECT NUMBER
	5e. TASK NUMBER
	5f. WORK UNIT NUMBER

7. PERFORMING ORGANIZATION NAME(S) AND ADDRESS(ES) **Sky Research, Inc,445 Dead Indian Memorial Road,Ashland,OR,97520**	8. PERFORMING ORGANIZATION REPORT NUMBER

9. SPONSORING/MONITORING AGENCY NAME(S) AND ADDRESS(ES)	10. SPONSOR/MONITOR'S ACRONYM(S)
	11. SPONSOR/MONITOR'S REPORT NUMBER(S)

12. DISTRIBUTION/AVAILABILITY STATEMENT
Approved for public release; distribution unlimited

13. SUPPLEMENTARY NOTES

14. ABSTRACT

15. SUBJECT TERMS

16. SECURITY CLASSIFICATION OF:			17. LIMITATION OF ABSTRACT	18. NUMBER OF PAGES	19a. NAME OF RESPONSIBLE PERSON
a. REPORT **unclassified**	b. ABSTRACT **unclassified**	c. THIS PAGE **unclassified**	**Same as Report (SAR)**	**39**	

Table of Contents

List of Figures

List of Tables

List of Acronyms

AIC	Akaike Information Criterion
APG	Aberdeen Proving Ground
BIC	Bayesian Information Criterion
BUD	Berkeley UXO Discriminator
cm	Centimeter
DLL	Dynamic Link Libraries
DoD	Department of Defense
EM	Electromagnetic
EMA	Expectation Maximization Algorithm
EMI	Electromagnetic Induction
ESTCP	Environmental Security Technology Certification Program
FCS	Former Camp Sibert
GSEA	Generalized standardized excitation approach
IDA	Institute for Defense Analyses.
JD	Joint Diagonalization
LBNL	Lawrence Berkeley National Laboratory
MEG	Magneto encephalographic
ML	Maximum Likelihood
μs	Microsecond
mm	Millimeter
MM	MetalMapper
MPV	Man-Portable Vector
ms	Millisecond
MR	Munitions response
MSR	Multi-static response
MUSIC	Multiple Signal Classification
NC	North Carolina
NSMS	Normalized surface magnetic source
NV/SMS	Normalized volume or surface magnetic source models
ONVMS	Orthogonal normalized volume magnetic source
ONV/SMS	Orthonormalized volume or surface magnetic source models
PNN	Probabilistic Neural Network
SERDP	Strategic Environmental Research and Development Program
SLO	San Luis Obispo
SVM	Support vector machine
TD	Time Domain
TEMTADS	Time Domain Electromagnetic Towed Array Detection System
TOI	Target of Interest
UXO	Unexploded Ordnance

1   INTRODUCTION

This demonstration is designed to illustrate the discrimination performance at a challenging live-site of advanced electromagnetic induction (EMI) modeling approaches, that are based on the normalized surface magnetic source NSMS model. The model is an extension of the simple dipole model, and provides better accuracy and discrimination ability. The approach combines 1. the NSMS for modeling targets EMI responses; 2. the differential evolution (DE) algorithm for nonlinear optimization to locate the target, and 3. Statistical classification approach for classifying targets as UXO and non-UXO. The study used cued data sets collected at San Luis Obispo, Calaifornia using three next-generation EMI sensors, the Geometrics MetalMapper (MM), the Time-domain Electro-Magnetic Towed Array Detection System (TEMTADS) developed by the NRL and G&G Sciences, and Berkley UXO Discriminator (BUD) developed at the Lawrence Berkeley National Laboratory (LBNL). The site was contaminated with 60 mm, 81 mm, 2.36 inch and 4.2 inch munitions. During this study, first targets extrinsic (location and depth) and intrinsic (the total NSMS, which depends on its size, shape and material properties) parameters were estimated from the data. Then, the inverted intrinsic parameters were used to classify the targets, and finally, sensor-specific dig-lists were generated for each EMI instrument and submitted to the Institute of Defense Analyses (IDA) for independent scoring.

1.1   Background

The Environmental Security Technology Certification Program (ESTCP) has recently launched a series of live-site UXO blind tests taking place in increasingly challenging and complex environments [1-4]. The first classification study was conducted in 2007 at the UXO live-site at the former Camp Sibert in Alabama using two commercially available first-generation EMI sensors (the EM61-MK2 and the EM-63, both from Geonics) [1]. At that site, the discrimination test was relatively simple: one had to discriminate large intact 4.2″ mortars from smaller range scrap, shrapnel and cultural debris, and the anomalies were very well separated.

The second ESTCP discrimination study took place in 2009 at the live-UXO site at Camp San Luis Obispo (SLO) in California and featured a more challenging topography and a wider mix of targets of interest (TOI) [4]. Magnetometers and first-generation EMI sensors (again the Geonics EM61-MK2) were deployed on the site and used in survey mode for a first screening. Afterwards, two advanced EMI sensing systems—the Berkeley UXO Discriminator (BUD) and the Naval Research Laboratory's TEMTADS array—were used to perform cued interrogation of a number of the anomalies detected. A third advanced system, the Geometrics MetalMapper, was used in both survey and cued modes for anomaly identification and classification. Among the munitions buried at SLO were 60-mm, 81-mm, and 4.2″ mortars and 2.36″ rockets.

1.2   Brief site history

Please refer to the ESTCP Live Site Demonstration Plan [3].

1.3   Objective of the demonstration

The advanced EMI models we present here (NSMS and JD) were developed under SERDP Project MM-1572 [5] and tested against TEMTADS data sets collected at the Aberdeen Proving Ground (APG) test site in Maryland [6-10]. The present test of discrimination performance considers data taken at SLO. This live site was contaminated with 60-mm, 81-mm, and 4.2″ mortars and 2.36″ rockets; and three additional types of munitions were discovered during the course of the demonstration.

Overall, the principal objective of this demonstration was to demonstrate the models' classification performance for live-site UXO problems. The specific technical objectives were to:

1. Demonstrate the classification accuracy of the NSMS model and its applicability to live-site UXO discrimination problems in terms of the signal to noise ratio and number of targets.
2. Illustrate and document the robustness of the data inversion and discrimination models.
3. Invert targets' intrinsic parameters and identify robust classification features.
4. Indentify all seeded and native UXO.
5. Indentify sources of uncertainty in the classification process and include them in a dig/no-dig decision process.
6. Understand and document the applicability and limitations of the advanced EMI discrimination technologies in the context of project objectives, number of targets, site characteristics, and suspected ordnance contamination.

2   TECHNOLOGY

The advanced EMI models and statistical signal processing approaches have been developed and tested under this SERDP Project MM-1572 [5]. Namely the methods were tested against the TEMTADS data sets from the APG test-site. The methods were able to detect and identify buried UXO ranging in caliber from 25 mm up to 155 mm. The technique was seen to be reasonably fast, accurate, and clutter-tolerant, and provided excellent classification in single-target scenarios when combined with multi-axis/transmitter/receiver sensors like TEMTADS [11]. To further evaluate the performance of this technology, in this work advanced EMI data inversion and classification studies are conducted for SLO, CA live-site.

We start our technology description with the overview of the NSMS (section 2.1), which we use to represent the signatures and extract the properties of subsurface targets in an efficient manner. In Section 2.2 we outline the Gaussian mixture model for target classification. In Section 2.3 we discuss the geometries and sensing modalities of the advanced EMI sensors, as well as the procedures we have in place to model the way the sensors establish primary fields and measure subsurface responses. We first describe the MetalMapper, and then continue with TEMTADS and BUD. Finally, in Section 2.4 we present the SLO data sets classification results obtained using the combined NSMS approach and advanced classification procedures.

2.1   The Normalized Surface Magnetic Source model

The most frequently used method for representing the EMI response of a metallic target in both frequency and time domains approximates the whole object with a set of orthogonal co-located point dipoles that fire up in response to the primary field; the induced dipole moment is related to the primary field through a symmetric polarizability tensor. The use of this dipole approximation is motivated by its speed and simplicity; this simplicity, however, rests on assumptions that often become problematic and limit the model's usefulness. One such assumption is that the buried target of interest is either far enough from the transmitter loop, or small enough, that the primary field is essentially uniform throughout its extent. Usually, complex targets composed of different materials and different sections that contribute appreciably to the response—and, in the case of UXO, containing such complicating features as fins and rings—simply cannot be modeled accurately with a single point dipole. Such cases require more advanced methods that will capture the underlying physics correctly. One such technique is the NSMS model.

The NSMS method [12-15] can be considered as a generalized surface dipole model, and indeed reduces to the point dipole model in a special limiting case. The NSMS approach models an object's response to the primary field of a sensor by distributing a set of equivalent elementary magnetic sources—normally oriented dipoles in this case—over an auxiliary surface that surrounds it. Such a surface distribution can be hypothetically generated by spreading positive magnetic charge over the outer side of the equivalent surface (usually a prolate spheroid) and an identical distribution of opposite sign on its inner side [16], resulting in a double layer of magnetic charge separated by an infinitesimal distance. This double layer introduces the proper discontinuities in the tangential components of the magnetic flux density vector **B** but does not affect the transition of its normal component, which must always be continuous given the lack of free magnetic charges in nature. The resulting magnetic-moment distribution radiates a field that

by construction satisfies the governing EMI equations and can thus account for the secondary field outside the object. The particulars of location and orientation are divided out by normalizing the dipole density at every point with the component of the primary magnetic field normal to the surface. The resulting surface amplitude Ω of the NSMS distribution is a property of the object, and its integral Q over the surface constitutes a sort of global magnetic polarizability that is independent of the computational constructs—primary field, surrounding surface, object location and orientation, etc.—introduced for its determination. The surface amplitude can be determined directly for library-matching purposes by minimizing the difference between measured and modeled data for a known combination of object and sensor at a given relative location and orientation.

The NSMS model is based upon the assumption that the entire scatterer can be replaced with a very thin auxiliary surface shell. The primary magnetic field strikes the shell and induces on it a surface magnetization. The normal component of the magnetic field flux is always continuous across a boundary (no free magnetic charges exist in the universe) between two media, the total scattered magnetic field can be represented with surface magnetic sources as

$$\mathbf{H}^{sc}(\mathbf{r}) = \oint_S \bar{\bar{G}}(\mathbf{r},\mathbf{r}') \cdot \mathbf{m}(s')ds' = \oint_S \bar{\bar{G}}(\mathbf{r},\mathbf{r}') \cdot \left[\bar{\bar{\mathbf{M}}}(s') \cdot \mathbf{H}^{pr}(s') \right] ds' \tag{1}$$

where

$$\bar{\bar{\mathbf{G}}}(\mathbf{r},\mathbf{r}') = \frac{1}{4\pi R^3} \left[\frac{3\mathbf{RR}}{R^2} - \bar{\bar{I}} \right], \quad \mathbf{R} = \mathbf{r} - \mathbf{r}'. \tag{2}$$

Thus the EMI response of a permeable and conducting metallic object can be represented using a surface density on magnetic dipoles $\mathbf{m}(s')$, that is proportional to a normalized surface distribution $\bar{\bar{\mathbf{M}}}(s')$ through

$$\mathbf{m}(s') \equiv \bar{\bar{\mathbf{M}}}(s') \cdot \mathbf{H}^{pr}(s') , \tag{3}$$

the integral of $\bar{\bar{\mathbf{M}}}(s')$ over the surface provides the total NSMS, $\bar{\bar{\mathbf{M}}}_{total} = \oint_S \bar{\bar{\mathbf{M}}}(s')ds'$, contains all the information about an object that could be of need in the UXO discrimination problem, incorporating the effects of heterogeneity, interaction with other objects, and near- and far-field effects.

2.2   Gaussian mixture models

2.2.1   Model-based supervised clustering

Targets of interest (TOI) with similar features (i.e., dipole polarizabilities or total NSMS) are likely to show similar power-law/exponential time decay patterns under various conditions, and as a result these patterns form clusters when plotted in a convenient and pertinent space. It is possible to identify an unknown target by comparing its time-decay parameters to those of a set of previously characterized, previously clustered objects and assigning it to the category where its profile fits best. Such "supervised" clustering allows the use of additional information from the training data as prior knowledge; on the other hand, it uses only the training set to estimate the parameters and completely ignores the blind data, which is potentially quite useful. The test

data set, moreover, is usually much larger than the training sample, implying that the unused information may be substantially richer than what is contained in the training sample.

Let us assume that there are K clusters and that each cluster is mathematically described by a parametric continuous or discrete distribution function (usually a Gaussian, as in this case). The classification parameters (extracted for example by fitting the total NSMS or ONVMS with a Pasion-Oldenburg time-decay law) can then be arranged in an $n \times m$ matrix denoted by $\mathbf{Y} = [\mathbf{Y}_1, \mathbf{Y}_2, \ldots, \mathbf{Y}_m]$, where $\mathbf{Y}_i$, $i = 1, 2, \ldots, n$, is a vector, n is the number of anomalies, and m is the number of parameters. Each $\mathbf{Y}_i$ can be considered to follow an m-dimensional mixture of normal distributions expressed as

$$F(\mathbf{Y}_i) = \sum_{k=1}^{K} w_k f_i(\mathbf{Y}_i \mid \boldsymbol{\mu}_k, \boldsymbol{\sigma}_k), \tag{4}$$

where w_k is the mixing weight of cluster k (defined as the proportion of anomalies that belong to it), $\Sigma_{k=1}^{K} w_k = 1$, and

$$f_i(\mathbf{Y}_i \mid \boldsymbol{\mu}_k, \boldsymbol{\sigma}_k) = \frac{1}{\sqrt{\boldsymbol{\sigma}_k (2\pi)^m}} \exp\left(-\frac{1}{2}(\mathbf{Y}_i - \boldsymbol{\mu}_k)' \boldsymbol{\sigma}_k^{-1}(\mathbf{Y}_i - \boldsymbol{\mu}_k) \right) \tag{5}$$

is the probability density of the k-th normal distribution with the $m \times 1$ mean vector $\boldsymbol{\mu}_k$ and the $m \times m$ variance-covariance matrix $\boldsymbol{\sigma}_k$. The parameters $\boldsymbol{\mu}_k$, $\boldsymbol{\sigma}_k$, and w_k are estimated by the maximum likelihood (ML) criterion using the Expectation Maximization (EM) algorithm.

This simple and intuitive supervised method usually performs well if the number of TOI within each known cluster in the training sample is sufficiently large to ensure high accuracy of the estimates of $\boldsymbol{\mu}_k$ and $\boldsymbol{\sigma}_k$. For small training samples these estimates are subject to large errors—in some cases, if the number of targets within a cluster is smaller than the number of parameters, the estimated variance-covariance matrices may not even be positive definite. Furthermore, much information from the test dataset has not been fully utilized. The test dataset is usually much larger than the training sample, implying that the unutilized information may be substantially more than that contained in the training sample. To overcome this problem we use unsupervised clustering and derive $\boldsymbol{\mu}_k$ and $\boldsymbol{\sigma}_k$ from blind-test data using an iterative EM algorithm.

2.2.2 *Unsupervised classification using the multivariate normal mixture approach*

Mixture distribution is perhaps the only model-based approach among existing methods of clusterization and pattern recognition. Its attractive features are that (a) it is not necessary to specify what class each observation belongs to (i.e., the classification is "unsupervised") and that (b) the method estimates the membership probability which results in *confusion matrix* $\boldsymbol{\pi}$.

Let $\mathbf{x}_1, \ldots, \mathbf{x}_n$ be m-dimensional feature vectors that we want to split into K classes. It is assumed that each $\mathbf{x}_i$ belongs to one of K classes that are described by densities $\varphi_1(\mathbf{x}), \ldots, \varphi_K(\mathbf{x})$. If $\pi_k \geq 0$

denotes the probability of $\mathbf{x}$ belonging to class k, then the mixture density is the linear combination

$$\varphi(\mathbf{x}) = \sum_{k=1}^{K} \pi_k \varphi_k(\mathbf{x}), \tag{6}$$

where

$$\sum_{k=1}^{K} \pi_k = 1. \tag{7}$$

In the case of a normal distribution we have

$$\sum_{k=1}^{K} \pi_k N(\mathbf{x}; \boldsymbol{\mu}_k, \boldsymbol{\Omega}_k) \tag{8}$$

for the mixture, where the mean $\boldsymbol{\mu}_k$ and the covariance matrix $\boldsymbol{\Omega}_k$ are different for the different clusters and subject to estimation along with probabilities π_k. Since the density of $N(\mathbf{x}; \boldsymbol{\mu}_k, \boldsymbol{\Omega}_k)$ is

$$\varphi_k(\mathbf{x}; \boldsymbol{\mu}_k, \boldsymbol{\Omega}_k) = (2\pi)^{-m/2} |\boldsymbol{\Omega}_k|^{-1/2} \exp\left[-\frac{1}{2} (\mathbf{x} - \boldsymbol{\mu}_k)' \boldsymbol{\Omega}_k^{-1} (\mathbf{x} - \boldsymbol{\mu}_k) \right], \tag{9}$$

the method of maximum likelihood prescribes the maximization of a nonlinear function:

$$L(\boldsymbol{\mu}_k \boldsymbol{\Omega}_k, \pi_k) = (2\pi)^{-m/2} \sum_{k=1}^{K} \pi_k |\boldsymbol{\Omega}_k|^{-1/2} \exp\left[-\frac{1}{2} (\mathbf{x} - \boldsymbol{\mu}_k)' \boldsymbol{\Omega}_k^{-1} (\mathbf{x} - \boldsymbol{\mu}_k) \right] \Rightarrow \max_{\boldsymbol{\mu}_k \boldsymbol{\Omega}_k, \pi_k} \tag{10}$$

This task is not easy because the function is unbounded (it may go to $+\infty$), and this creates numerical obstacles. The expectation-maximization (EM) algorithm is used to determine $\pi_k, \boldsymbol{\mu}_k, \boldsymbol{\Omega}_k$ as follows:

1. Let the initial estimates of $\pi_k, \boldsymbol{\mu}_k, \boldsymbol{\Omega}_k$ be given (for example, we can take $\pi_k = 1/K$, $\boldsymbol{\Omega}_k = \mathbf{S}_x$, and $\boldsymbol{\mu}_k$ from K).

2. Compute the elements of the confusion matrix $\boldsymbol{\pi}$ as the probability that a given observation $\mathbf{x}_i$ belongs to class k:

$$\pi_{ik} = \frac{\pi_k \varphi_k(\mathbf{x}; \boldsymbol{\mu}_k, \boldsymbol{\Omega}_k)}{\sum_{j=1}^{K} \varphi_j(\mathbf{x}; \boldsymbol{\mu}_j, \boldsymbol{\Omega}_j)}. \tag{11}$$

3. Adjust the probabilities accordingly:

$$\pi_k = \frac{1}{n} \sum_{i=1}^{n} \pi_{ik}. \tag{12}$$

4. Recompute the means

$$\boldsymbol{\mu}_k = \frac{\sum_{i=1}^{n} \pi_{ik} \mathbf{x}_i}{n \pi_k} \tag{13}$$

and covariance matrices

$$\boldsymbol{\Omega}_k = \frac{2 a_n \mathbf{S}_x + \mathbf{S}_k}{2 a_n + n \pi_k}, \tag{14}$$

where:

$$\mathbf{S}_k = \sum_{i=1}^{n} \pi_{ik} (\mathbf{x}_i - \boldsymbol{\mu}_k)(\mathbf{x}_i - \boldsymbol{\mu}_k)' . \tag{15}$$

5. If the values are different from the previous iteration return to Step 1 and continue until reaching convergence.

2.3   Modeling of advanced EMI systems

A wide range of different electromagnetic induction sensing technologies, with novel waveforms, multi-axis transmitters, and scalar/vector receivers have been recently developed under SERDP-ESTCP programs. These advanced EMI sensors—including the MetalMapper, the TEMTADS array, and the Berkeley UXO discriminator (BUD) provide measurements that feature a combination of high spatial diversity, different viewpoints, and a very wide dynamic range and which do full justice to the vector character of the electromagnetic field.

2.3.1   MetalMapper

The MetalMapper (MM) is an advanced EMI system for UXO detection and discrimination developed primarily by G&G Sciences and commercialized by Geometrics. The system has three mutually orthogonal transmitter rectangular loops. It is able to illuminate a target with primary fields from three independent directions from a single spatial field point. The $1\,\mathrm{m} \times 1\,\mathrm{m}$ Z transmitter loop is located at ground level. The Y transmitter loop, also $1\,\mathrm{m} \times 1\,\mathrm{m}$, is centered 56 cm above the Z loop, as is the $0.98\,\mathrm{m} \times 0.98\,\mathrm{m}$ X transmitter (Figure 1). The targets are illuminated from different directions depending on the geometry between a particular transmitting loop and the target. The system has seven 10-cm-side receiver cubes placed at seven unique spatial points on the plane of the Z transmitter loop. The receivers measure the vector $d\mathbf{B}/dt$ at each of the seven points, thus providing 63 independent readings of the transient secondary magnetic field for each instrument location. The positions of the receiver cubes' centers with respect to the Z transmitter loop (whose center we consider as the local origin of coordinates for the system) are given in Table 1.

Figure 1: The MetalMapper during SLO site deployment (left) and its schematic diagram (right).

Table 1: MetalMapper receiver locations with respect to the center of the *Z* transmitter loop.

Rx #	X [cm]	Y [cm]	Z [cm]
0	39	39	5
1	−26	26	5
2	13	13	5
3	0	0	5
4	−13	−13	5
5	26	−26	5
6	−39	−39	5

The MM transmitters are modeled as infinitely thin rectangular wires. The primary magnetic induction produced at any observation point **r** by the *T*-th loop is determined simply from the Biot-Savart law,

$$\mathbf{B}_T(\mathbf{r}) = \frac{\mu_0}{4\pi} \sum_{i=1}^{N_{Tx}} \frac{I_T[\Delta\boldsymbol{\ell}_{T,i} \times \mathbf{R}_{T,i}]}{R_{T,i}^3}, \quad T = 1, 2, 3, \tag{16}$$

where, $\mathbf{R}_{T,i} = \mathbf{r} - \mathbf{r}'_{T,i}$, $\mathbf{r}'_{T,i}$ is the location of the *i*-th current element, and $\Delta\boldsymbol{\ell}_{T,i}$ is the tangential length vector for the *i*-th subsection of the Tth loop. In what follows, and unless we note otherwise, we divide each transmitter coil into $N_{Tx} = 40$ subsections whenever we calculate the primary magnetic induction using Eq. (16).
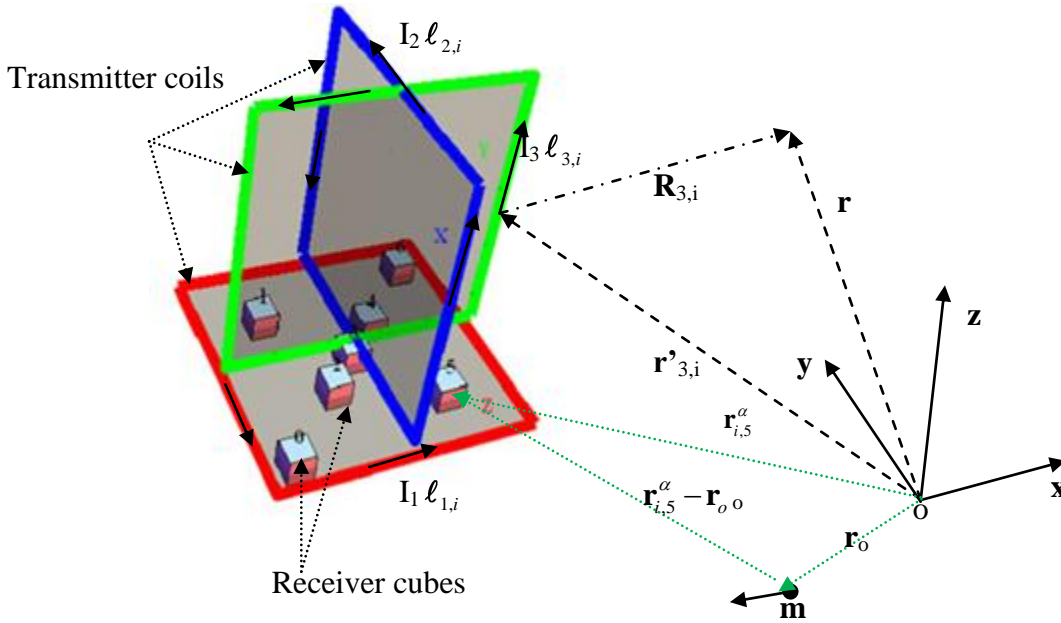
Figure 2. The MetalMapper geometry. The observation point **r** is defined with respect to the global Cartesian coordinate system XYZO; $\mathbf{r}'_{3,i}$ is the location of the i-th current element on (in this case) the $T = 3$ transmitter, which carries a current I_3 in the direction $\ell_{3,i}$.

The MM receiver assembly consists of seven cube sensors. Each of these measures along three orthogonal directions the induced voltages that, from Faraday's law, correspond to the negative of the time derivative of the secondary magnetic flux through the area spanned by the different coils. The induced voltage in the R-th sensor along the α-th direction, where $R = 0,\ldots,6$ and $\alpha = z, y, x$, is computed using

$$V_R^\alpha = -\int_{S_R^\alpha} \frac{\partial \mathbf{B}}{\partial t} \cdot d\mathbf{s}_R^\alpha = \sum_{i=1}^{N_{Rx}} \frac{\partial \mathbf{B}_i(\mathbf{r}_{i,R}^\alpha - \mathbf{r}_o)}{\partial t} \cdot \hat{\mathbf{n}}_\alpha \ \Delta s_{i,R}^\alpha , \tag{17}$$

where s_R^α is the area of the relevant coil (all of which are $10\,\text{cm} \times 10\,\text{cm}$ squares in MetalMapper) and $\hat{\mathbf{n}}_\alpha$ is the unit vector perpendicular to it, $\Delta s_{i,R}^\alpha$ and $\mathbf{r}_{i,R}^\alpha$ are respectively the i-th sub-area and vector location point on s_R^α, $\mathbf{B}_i(\mathbf{r}_{i,R}^\alpha) = \mu_o \mathbf{H}_i(\mathbf{r}_{i,R}^\alpha)$ is the magnetic induction (proportional to the magnetic field $\mathbf{H}_i(\mathbf{r}_{i,R}^\alpha)$) produced at $\mathbf{r}_{i,R}^\alpha$ by a source placed at $\mathbf{r}_o$. Within the NSMS model, $\mathbf{H}_i(\mathbf{r}_{i,R}^\alpha)$ is calculated using equation (1) in section 2.1. In what follows we always divide s_R^α into $N_{Rx} = 4$ sub-areas.
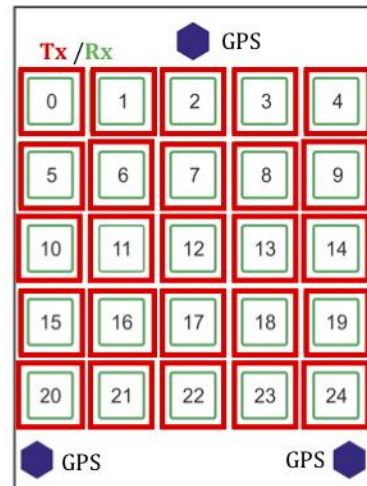
Figure 3: Photo of the TEMTADS in deployment at APG site (left) and a schematic diagram of its Tx/Rx sensors (right).

2.3.2   TEMTADS

The NRL time-domain EMI sensor array TEMTADS is a next-generation system designed for subsurface target discrimination. The sensor consists of 25 transmit/receive pairs, each composed of a 35-cm square transmitter loop surrounding a 25-cm square receiver loop, arranged in a rectangular 5×5 grid with 40-cm neighbor-to-neighbor separation [11] (Figure 3). The sensor activates the transmitter loops in sequence, one at a time, and for each transmitter all receivers receive, measuring the complete transient response over a wide dynamic range of time going approximately from 100 microseconds (μs) to 25 milliseconds (ms) and distributed in 123 time gates. The sensor thus provides 625 spatial data points at each location, with unprecedented positional accuracy.

In modeling for TEMTADS, the transmitter loops are idealized as infinitesimally thin $35 \text{ cm} \times 35 \text{ cm}$ square loops. The primary field produced at any observation point by a given transmitter loop is determined from equation (16). We use $N_{Tx} = 20$ for TEMTADS unless we note otherwise. The TEMATDS measured signal is modeled using equation (17), assuming $\alpha = z$ throughout and receiver sizes of 25 cm × 25 cm and dividing each receiver into $N_{Rx} = 9$ sub-areas.
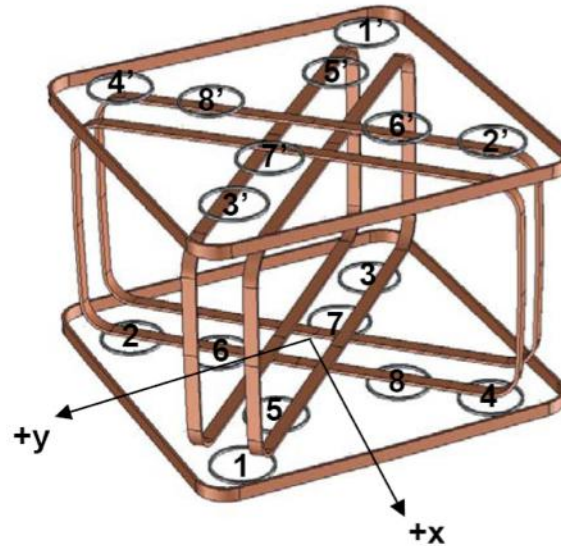
Figure 4: Schematic diagram of the BUD system.

2.3.3   BUD

The Berkeley UXO discriminator (BUD) is an advanced standalone time-domain system developed at the Lawrence Berkeley National to detect and discriminate UXO in the 20-mm to 155-mm size range, and consists of three orthogonal coil transmitters. The horizontal *Z*-coils are vertically separated by 26″ and have a 39″ × 39″ footprint. The *Y*- and *X*-vertical coils are mounted on the diagonals between the *Z*-coils (see Figure 4): the *X*-coils are 45.5″ × 23.5″ while the *Y*-coils are 45.5″ × 22.5″ in size, and both are separated by 6″. The BUD illuminates targets in three independent directions, which induce eddy currents in all three modes. BUD has eight pairs of differenced receiver coils placed horizontally along the two diagonals of the upper and lower planes of the *Z*-transmitter loops. The pairs are located on symmetry lines trough the center and are wired in opposition so as to cancel the primary magnetic field during transmission. Figure 5 shows the BUD system in operation.

The BUD transmitter loops were modeled as idealized infinitely thin square loops. The primary fields produced at any observation point by the transmitters are determined using a suitable modification of equation (16), again with $N_{Tx} = 40$. The BUD measured signals are modeled using equation (17) as

$$V_R = -\sum_{i=1}^{N_{Rx}} \frac{\partial \mathbf{B}_i(\mathbf{r}_{i,R} - \mathbf{r}_0)}{\partial t} \cdot \Delta \mathbf{s}_{i,R} + \sum_{i=1}^{N_{Rx}} \frac{\partial \mathbf{B}_i(\mathbf{r}'_{i,R} - \mathbf{r}_0)}{\partial t} \cdot \Delta \mathbf{s}_{i,R}, \quad \Delta \mathbf{s}_{i,R} = \Delta s_{i,R} \hat{\mathbf{z}} \tag{18}$$

where $\mathbf{r}_{i,R}$ and $\mathbf{r}'_{i,R}$ are the locations of the Rx and Rx′ receivers, given in Table 2. For the case of BUD we divide the receivers into $N_{Rx} = 9$ sub-areas.
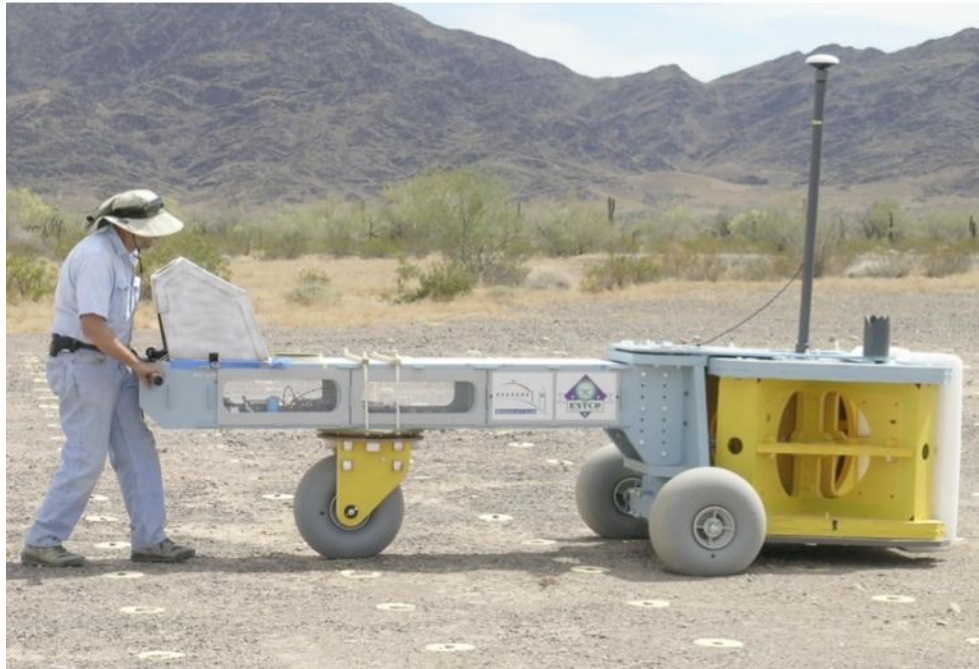
Figure 5: The BUD system in operation.

Table 2: BUD receiver locations with respect to the origin.

Rx #	X [cm]	Y [cm]	Z [cm]	Rx' #	X'[cm]	Y'[cm]	Z'[cm]
1	35.48	35.48	0	1'	−35.48	−35.48	66
2	−35.48	35.48	0	2'	35.48	−35.48	66
3	−35.48	−35.48	0	3'	35.48	−35.48	66
4	35.48	−35.48	0	4'	−35.48	35.48	66
5	19.29	19.29	0	5'	−19.29	−19.29	66
6	−19.29	19.29	0	6'	19.29	−19.29	66
7	−19.29	−19.29	0	7'	19.29	19.29	66
8	19.29	−19.29	0	8'	−19.29	19.29	66

2.4   SLO data sets classification results

Our group conducted SLO classification studies using the advanced EMI models. Namely, the combined NSMS-DE algorithm was used for data inversion and classification parameter extractions, and library matching and Gaussian mixture models were used for classification. Each anomaly was treated as a single well separated target, i.e. no multi-target scenarios were considered. The target response was approximated with set of magnetic dipoles distributed on a spherical surface of radius 5 cm. This sphere is divided into 17 subsurfaces, each of which is assumed to contain a magnetic-dipole distribution of constant density. Once the location of the sphere's center is determined then the magnitude of each responding source is obtained and the total NSMS is calculated. The SERDP Program Office provided us with training data sets for the analysis of the algorithms testing performance.

2.4.1   SLO TEMTADS Classification

The SERDP office provided us the 188 TEMTADS calibration data, that we used to build a library of the expected total NSMS values for TOI. This library was then used on the rest 1282 test cells for classifying anomalies as TOI-and non-TOI-s. We used all 115 TEMTADS time channels that span, in approximately logarithmic fashion, a lapse of time between 100 μs and 24 ms. The inversion code assumed that the TEMTADS instrument was always placed 30 cm above the ground.

For each data set we run the combined NSMS-DE to estimate object extrinsic (locations and depth) and intrinsic (total NSMS) parameters. The inverted total NSMS curves for SLO TEMTADS calibration (green lines) and blind data sets (red lines) are depicted in Figure 6 and Figure 7 for partial 2.36″ rockets, 4.2″ mortars, 81-mm projectiles, 2.36″ rockets, and 60-mm mortars. The results indicate that the inverted and calibration total NSMS time decay curves are similar and are good discriminators. Also, as the size of the TOI decreases the inverted total NSMS time decay curves show a larger spread, making them harder to discriminate.
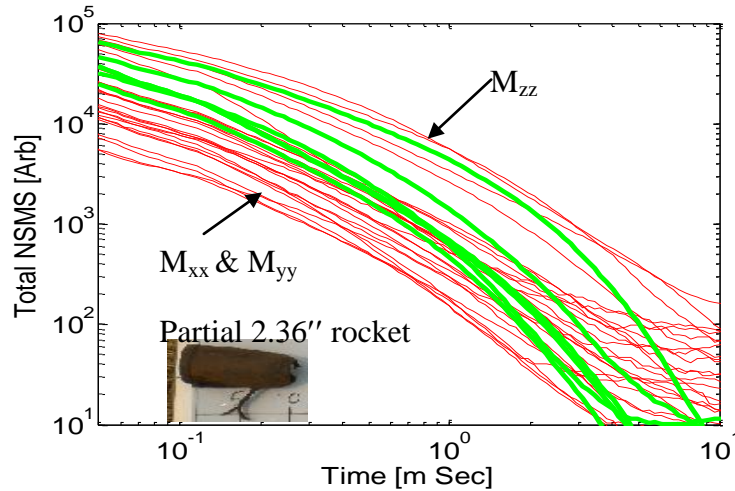
Figure 6: Inverted total NSMS time decay profiles for the 2.36″ partial rocket. The green lines depict calibration data and the red lines correspond to blind SLO TEMTADS data sets.
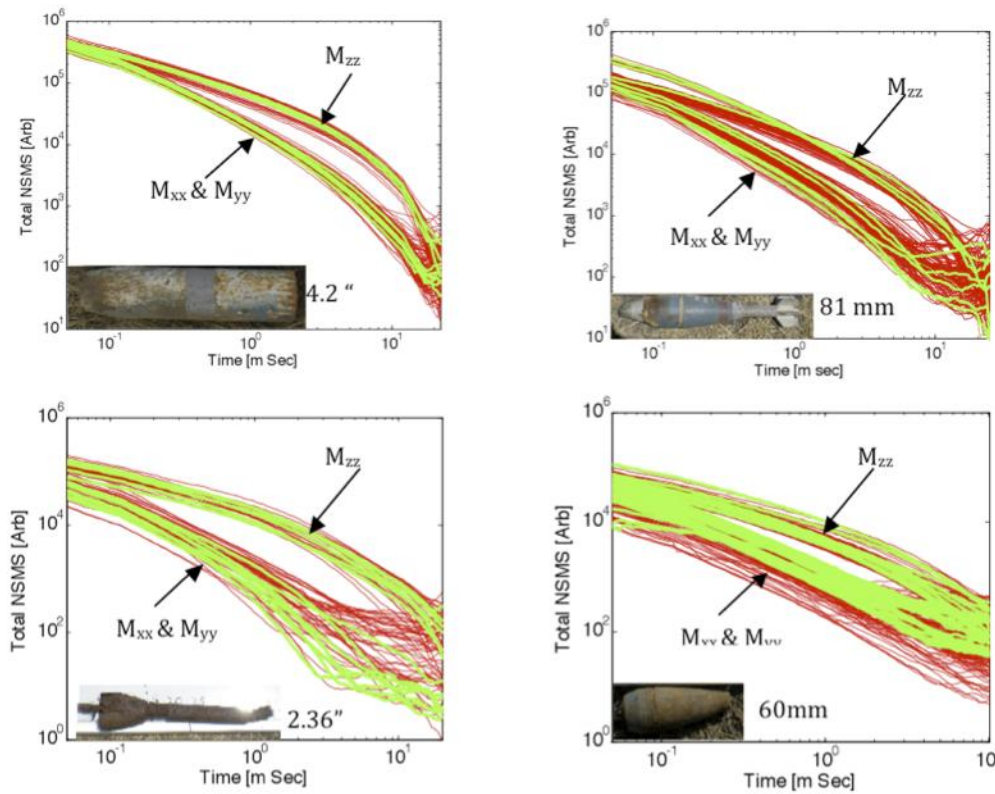
Figure 7: Inverted total NSMS time decay profiles for 4.2″ mortars (top left), 81-mm projectiles (top right), 2.36″ rockets (bottom left), and 60-mm mortars (bottom right) in the SLO TEMTADS test. The green lines depict calibration data and the red lines correspond to blind data sets.
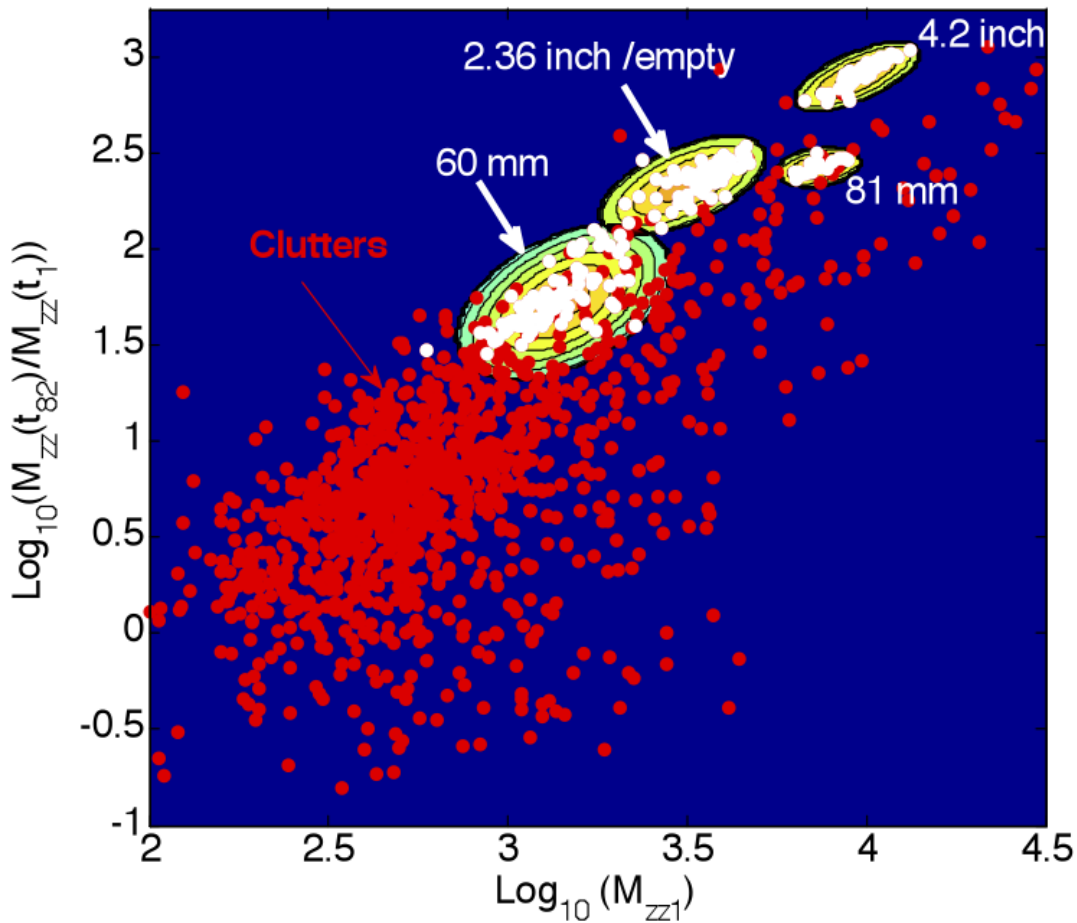
Figure 8: Result of the supervised clustering classification for the SLO-TEMTADS anomalies using the logarithms of $M_{\alpha\alpha}(t_1)$ and $M_{\alpha\alpha}(t_1)/M_{\alpha\alpha}(t_{80})$. The supervised clustering has been trained with calibration data. The red markers correspond to clutters and the white ones to TOI.

Once the total NSMS were determined, the values of $\log_{10}(M_{\alpha\alpha}(t_1)/M_{\alpha\alpha}(t_{80}))$ versus $\log_{10}(M_{\alpha\alpha}(t_1))$ were extracted for each anomaly, and semi-supervised Gaussian mixture model was used to classify the targets as TOI-and non-TOI. These values are plotted in Figure 8 for all TEMTADS data sets as red and white dots. In addition, Figure 8 shows distribution of the Gaussian mixture classification function (color map distributed between blue (zero level) and red (maximum value, one) colors). We see that the inverted parameters are well clustered, and, those of TOI are noticeably distinct from all others, suggesting that this two-dimensional feature space should provide good classification.

We combined the Gaussian mixture model and library matching classification results and built a dig list. The dig list was submitted to the IDA for scoring. The scored results in ROC curve form are depicted for all TOI and individual TOI-s in Figure 9 and Figure 10.
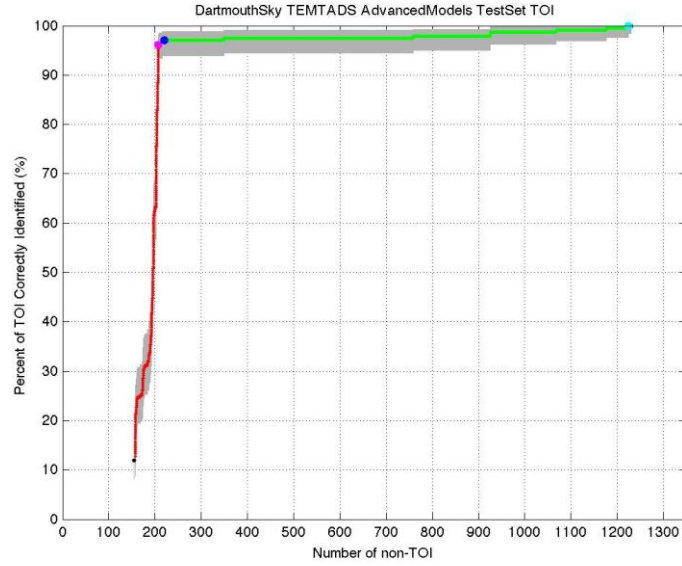
Figure 9: ROC curve for SLO TEMTADS test data.
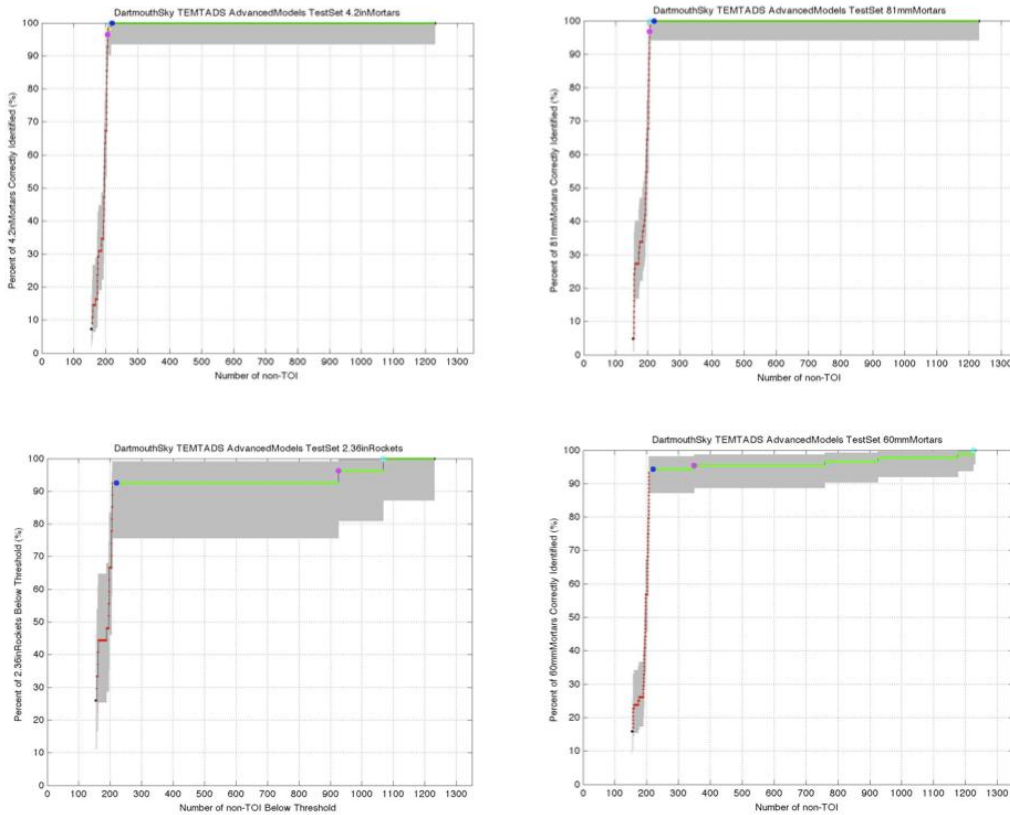
Figure 10: ROC for SLO TEMTADS data for individual TOI.

The results show that our classification approach was able to correctly identify most TOI. It was able to classify large 4.2" and 81 mm mortars and well-separated 2.36 " rockets, 60 mm mortars, which produced high signal to noise ratios. It had difficulties to tag correctly two 2.36″ rockets and five 60-mm mortars, which were mostly placed with other targets or had small signal-to-noise ratios.

2.4.2   SLO MM Classification

The SERDP office provided us 2492 SLO cued MM data sets. Each data set was inverted using the combined NSMS-DE algorithm for single objects. to extract the extrinsic and intrinsic parameters of the targets. The extracted intrinsic parameters (NSMS) were used to classify targets as UXO and non-UXO targets and a prioritized dig list was created. The dig list was then submitted to the SERDP office for independent scoring, which was carried out by personnel from the Institute for Defense Analyses (IDA). Our discrimination results are summarized in Figure 11 and Figure 12. Our classification technique was able to correctly identify all big UXO, (the 2.36″, 81-mm and 4.2″ projectiles) for MetalMapper data. The algorithm missclassified only one seeded 60-mm mortar, MM anomaly# 1285. The missed TOI was buried at 35 cm depth, and the inverted total NSMS for the anomaly are significantly different compared to the total NSMS for a library 60 mm mortar, Figure 13. Based on these differences, the anomaly #1285 was ranked as non-TOI target.
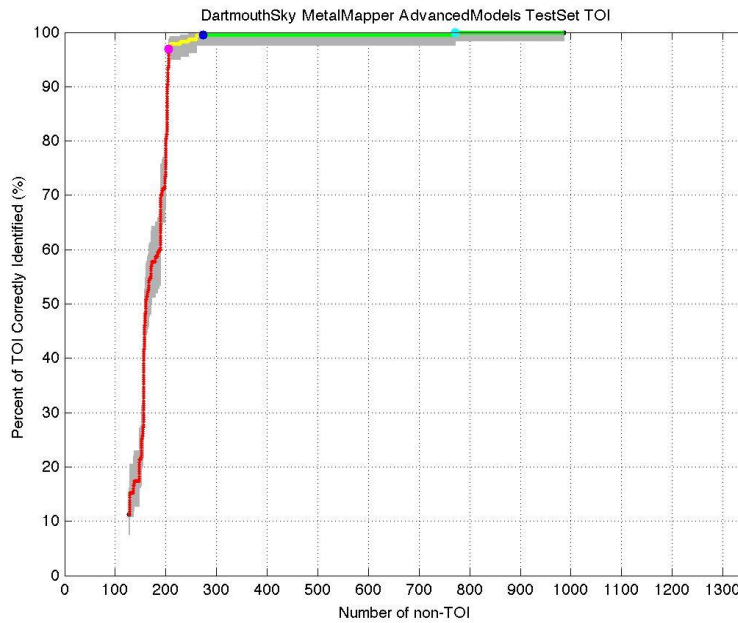
Figure 11: ROC curve for SLO MetalMapper test data.
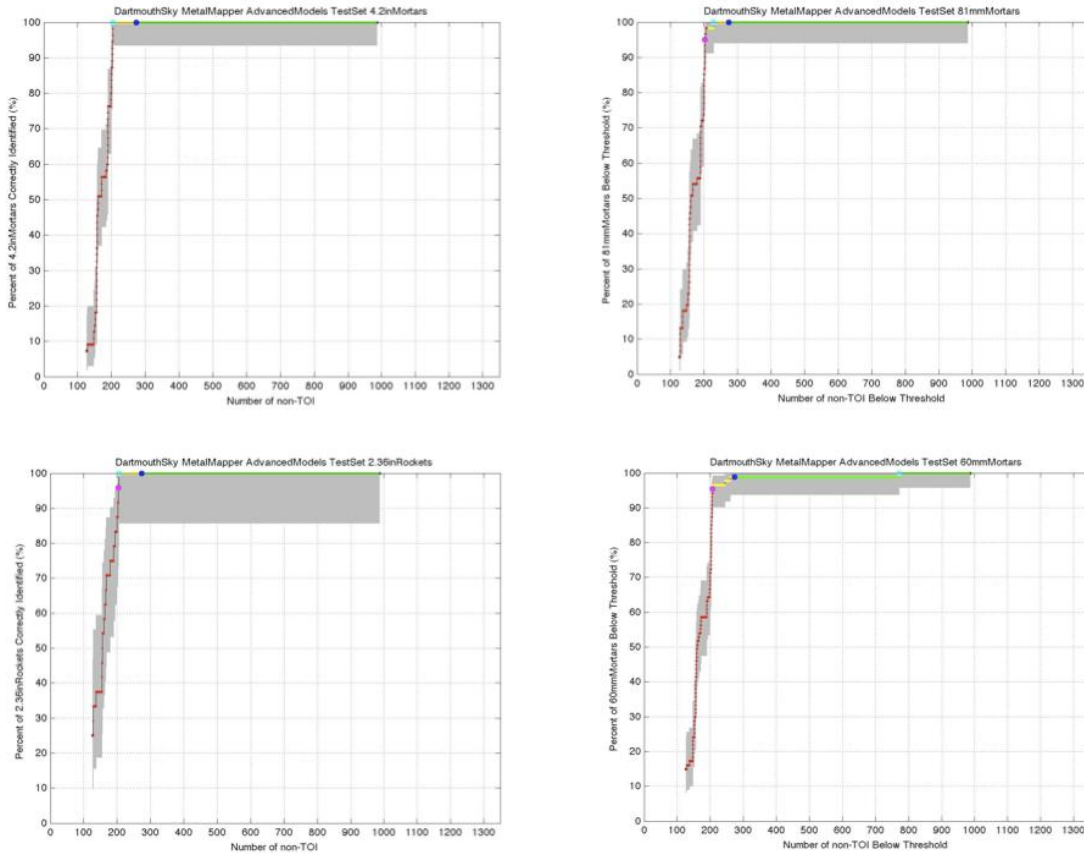
Figure 12: ROC curve for SLO MetalMapper data sets: individual TOI.
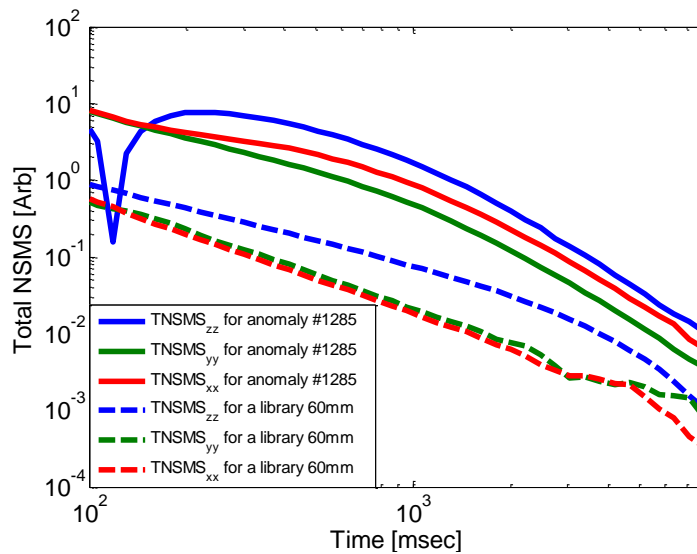
Figure 13: The total NSMS for MM anomaly #1285 (solid lines) and a library 60 mm mortar (dashed lines).
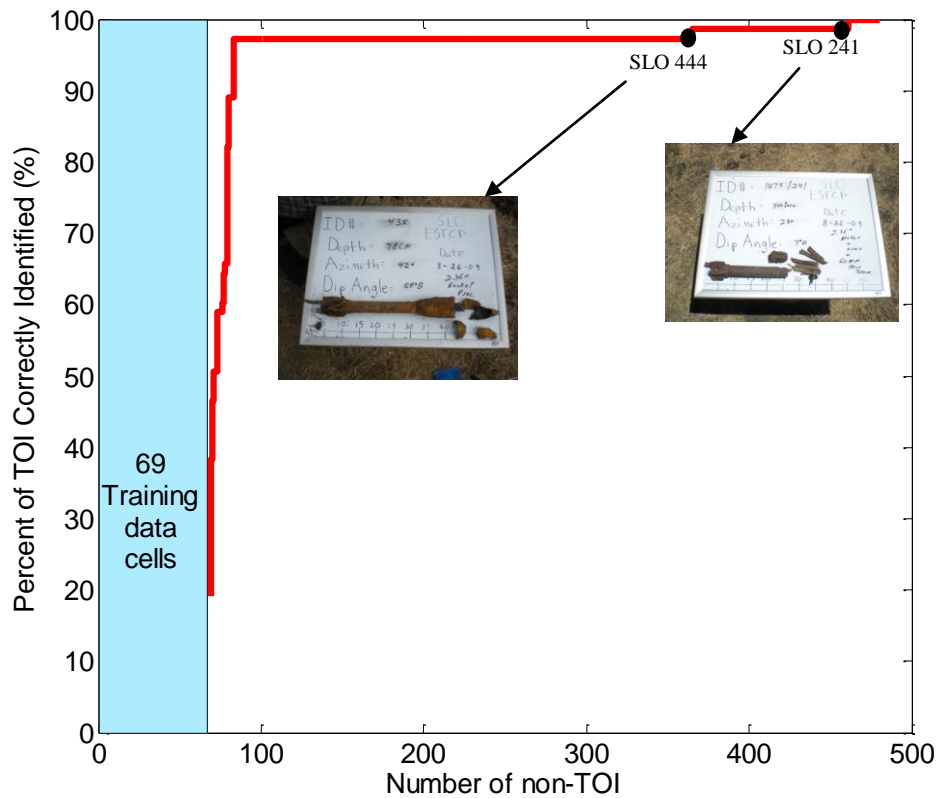
Figure 14: ROC curves for SLO BUD discrimination studies.

2.4.3   *SLO BUD data inversion and classification studies*

The SERDP office also provided SLO BUD data sets (total 539 anomalies) for assessing our technology for the BUD system. We adapted NSMS_DE approach to the BUD data sets and applied it to first the SLO training data sets (in total 69) and then to SLO live site BUD data. We extracted targets intrinsic (total NSMS) and extrinsic parameters for each of the anomalies. The discrimination features (size and shape information) were extracted from the total NSMS time decay curve and anomalies were classified using the library matching and Gaussian mixture model. The inverted targets were ranked as TOI and non-TOI items. The ROC curve for the SLO BUD data sets that was ranked independently in our group, is shown in Figure 14. The studies showed that only 2.36 inch rockets were misclassified. In both cases the signals from the missed targets were contaminated with signals from nearby non-UXO.

3   PERFORMANCE OBJECTIVES

The performance objectives of this ESTCP live site discrimination study were: to achieve high probability of discrimination of UXO from among a wide spread of clutter; to process all data sets; to minimize the number of data that could not be analyzed or decided upon; to minimize the number of false positives; and to identify all UXO with high confidence. The performance objectives are summarized in Table 3.

Table 3: Performance objectives

Performance Objective	Metric	Data Required	Success Criteria
Maximize correct classification of munitions	Number of targets-of-interest retained	• Prioritized anomaly lists • Scoring reports from Institute for Defense Analysis (IDA)	Approach correctly classifies all targets-of-interest
Maximize correct classification of non-munitions	Number of false alarms eliminated	• Prioritized anomaly lists • Scoring reports from IDA	Reduction of false alarms by > 75% while retaining all targets of interest
Specification of no-dig threshold	Probability of correct classification and number of false alarms at demonstrator operating point	• Demonstrator - specified threshold • Scoring reports from IDA	Threshold specified by the demonstrator to achieve criteria above
Minimize number of anomalies that cannot be analyzed	Number of anomalies that must be classified as "Unable to Analyze"	• Demonstrator target parameters	Reliable target parameters can be estimated for > 90% of anomalies on each sensor's detection list.
Correct estimation of target parameters	Accuracy of estimated target parameters	• Demonstrator target parameters • Results of intrusive investigation	Total NSMS ± 10%

3.1   Objective: maximize correct classification of munitions

An effective technology for discrimination of munitions should maximize the number of targets of interest (TOI) it can classify as such (thus distinguishing them from non-TOI) with high confidence.

3.1.1   Metric

Identify all seeded and native TOI with high confidence using advanced EMI discrimination technologies. Our estimates, for "High confidence", were based on using the extracted total NSMS as input to statistical classification algorithms and expert judgment. Every anomaly that was close to a TOI cluster in feature space (Figure 8) and had $f > 10^{-7}$, where f is the probability density function of equation (5), was considered to be a possible TOI; the expert then inspected the corresponding TNSMS curve for symmetry (manifested by equal secondary and tertiary TNSMS) and signal-to-noise ratio.

3.1.2   Data requirements

We analyzed data from three instruments, the 5×5 TEMTADS array, the MetalMapper and BUD. For each sensor we used supplied training data sets. The training data were used to validate the models for each specific sensor. We generated dig-lists that were scored by the IDA for TEMTADS and MM, and by ourselves for BUD test anomalies , respectively. Our studies showed that the supplied training data provided a little or no critical information for targets classification; Therefore, we suggested to use a custom training data set for future classification studies.

3.1.3   Success criteria evaluation and results

The objective was considered to be met if all seeded and native UXO items could be identified below an analyst-specified no-dig threshold.

3.1.4   Results

The objective was not met. Our algorithms classified most TOI correctly, however missed seven, one and two TOI for TEMTADS, MM and BUD sensors, respectively. Retrospective analysis showed that missed targets were in multi-target environment(see Figure 14), or buried deep and had small SNR.

3.2   Objective: maximize correct classification of non-munitions

The technology aims to minimize the number of false negatives, i.e., maximize the correct classification of non-TOI.

3.2.1   Metric

We compared the number of non-TOI targets that can be left in ground with high confidence using the advanced EMI discrimination technology to the total number of false targets that would be present if the technology were absent.

3.2.2   Data requirements

This objective required prioritized anomaly lists, which our team generated independently for each sensor, and for its evaluation we needed scoring reports from the IDA or ground truth from the SERDP office for retrospective studies.

3.2.3   Success criteria evaluation and results

The objective was considered to have been met if the method eliminated at least 75% of targets that did not correspond to TOI in the discrimination step.

3.2.4   Results

This objective was not met. In this study, only single object NSMS-DE algorithm was used for targets parameters inversion and classification. The classification algorithm was unable to classify all TOI-s correctly, particularly in case of multi targets and when targets were buried deep i.e. small SNR. To overcome these problems in the future, we developed the ortho-normalized volume magnetic source (ONVMS) and the joint diagonalization (JD) techniques for modeling multi targets response and estimating number of potential targets. The ONVMS and JD techniques were successfully demonstrated during camp Butner, NC [17] and Camp Beale, CA [17] ESTCP classification studies.

3.3   Objective: specify a no-dig threshold

This project aims to provide a high-confidence classification approach for UXO-site managers. A critical quantity for minimizing the residual risk of UXO and providing regulators with acceptable confidence is a specific no-dig threshold.

3.3.1   Metric

We compared an analyst's no-dig threshold point to the point where 100% of munitions were correctly identified.

3.3.2   Data requirements

To meet this requirement we needed scoring reports from the IDA.

3.3.3   Success criteria evaluation and results

The objective would be met if a sensor-specific dig list placed all the TOI before the no-dig point and if additional digs (false positives) were requested after all TOI were identified correctly.

3.3.4   Results

This objective was not met successfully for all data sets. The stop-dig thresholds, based on the library matching and Gaussian mixture model were specified at the point before all TOI were identified. Our retrospective studies showed that the missclassified TOI were surrounded by other targets, or had small SNR.

3.4   Objective: minimize the number of anomalies that cannot be analyzed

Some anomalies may not be classified, either because of the data are not sufficiently informative—the sensor physically cannot provide the data to support classification for a given target at a given depth—or because the data processing was inadequate. The former is a measure of instrument performance for all anomalies for which all data analysts converge. The latter is a measure of the quality of a data analysis, when a target diagnostic differs from those made by other analysts.

3.4.1   Metric

The metric for this objective is the number of anomalies that cannot be analyzed by a particular method, and the intersection of all anomaly lists among all analysts.

3.4.2   Data requirements

Each analyst submitted their anomaly list. IDA scored all lists and returned a list of anomalies that could not be analyzed by any analyst ("cannot analyze" or "failed classification").

3.4.3   Success criteria evaluation and results

The objective was met if at least 95% of a set of selected anomalies could be analyzed.

3.4.4   Results

This objective was successfully met. All four data sets for all anomalies were analyzed. Not a single anomaly was ranked as "cannot analyze."

3.5   Objective: correct estimation of target parameters

The combined NSMS-DE algorithm provides intrinsic and extrinsic parameters for the different targets. The intrinsic parameters were used for classification, while the extrinsic parameters (i.e., the target locations) were utilized for inversion algorithms assessment.

3.5.1   Metric

The classification results entirely depend on how accurately these parameters are estimated.

3.5.2   Data requirements

To achieve this objective we inverted and tabulated the intrinsic and extrinsic parameters for all targets. To validate extracted extrinsic parameters we needed results of intrusive investigations.

3.5.3   Success criteria evaluation and results

The objective was met if the targets' intrinsic parameters varied within $\pm10\%$.

3.5.4   Results

Estimated Classification parameters for large TOIs were varied within $\pm$ 10 %. Similar trends were achieved for most middle-size TOI-s in cases of high SNR, but the trend diverged for small SNR cases. These studies indicated that more noise-tolerant approaches were needed for live site UXO classification. We responded to this by extending the NSMS model to the ONVMS model and adapting the JD technique for data pre-processing.

4   TEST DESIGN

The only required test at the SLO site entailed collecting training data for target characterization: Using a calibration pit, the data-collection team made a series of static measurements of example targets at several depths and attitudes in order to cross-check models, confirm Tx and Rx polarity for the sensors, and characterize the so-called "library targets."

4.1   Site preparation

N/A

4.2   Demonstration schedule

Tasks and demonstration stages	Preparation Calibration	Blind data set			Post-survey analysis		
	Aug2009	Sep '09	Oct '09	Nov '09	Dec '09	Jan '10	Feb '10
1. Invert all calibration and training data	x						
2. Invert 5 × 5 TEMTADS data		x					
3. Invert MM data		x					
4. Generate MM dig list and submit to IDA				x			
5. Generate TEMTADS dig list and submit to IDA				x			
6. Invert BUD data and generate dig list					x		
7. Conduct retrospective analysis if needed						x	x
REPORTING:							
8. Draft demonstration report						x	
9. Final demonstration report							x

Figure 15. Gantt chart showing a detailed schedule of the activities conducted at SLO.

5   DATA ANALYSIS PLAN

We analyzed all cued data for the MetalMapper, TEMTADS and BUD sensors and produced prioritized dig lists for independent scoring.

5.1   Extracting target locations

Target locations were determined relative to the sensor coordinate system using the differential evolution and gradient descent search algorithms. Object responses were modeled with NSMS. This combined algorithm was run for single-target cases and provided target locations.

5.2   Extracting target intrinsic parameters

The NSMS algorithm yields the targets' intrinsic total NSMS, which we used for classification. The total NSMS contains three moments, $M_{xx}(t)$, $M_{yy}(t)$, and $M_{zz}(t)$, along the primary axes in the target's own reference frame. These moments are similar to simple dipole moment components but carry more information, accounting for the targets' inherent heterogeneities. The NSMS-DE algorithm outputs the time-decay curves of the target's total ONVMS tensor $M_{ij}(t_k)$. The next step is to determine the time decay of the primary components of the total NSMS in the target's reference frame. While this can be done by standard diagonalization (i.e., finding $\mathbf{M}(t_k) = \mathbf{V}(t_k)\mathbf{D}(t_k)\mathbf{V}^T(t_k)$, where $\mathbf{V}(t_k)$ contains the eigenvectors of $\mathbf{M}(t_k)$, it is more convenient to perform a joint diagonalization, $\mathbf{M}(t_k) = \mathbf{V}\mathbf{D}(t_k)\mathbf{V}^T$, where now the eigenvectors are shared by all time channels; this allows us to extract more reliable total NSMS values and reduce uncertainty.

5.3   Selection of intrinsic parameters for classification

Most UXO are bodies of revolution, and consequently the two secondary polarizability elements are degenerate. However, live-site UXO discrimination studies have repeatedly shown that this symmetry can be compromised due to low SNR, especially for small or deep targets. A good classification of object features can then be obtained by using only the principal component of the total NSMS, $M_{zz}(t)$. Furthermore, to limit the number of relevant features for use in classification we extract parameters exclusively from the main polarizability $M_{zz}(t)$, both to represent size (via $M_{zz}(t_1)$) and wall thickness (via $M_{zz}(t_1) / M_{zz}(t_n)$).

5.4   Training

We used the supplied training data set for algorithm training and optimization. At the first stage of the process we used a semi-supervised clustering technique to identify potential site-specific TOI.

5.5   Classification

(a) Probability density functions were extracted for single targets.

(b) All of the unknown targets were scored based on the probability density functions.

(c) All items were further analyzed using library matching, and all total NSMS time-decay curves were inspected visually.

(d) A classification threshold was selected and a final dig list was produced.

5.6   Decision memo

The algorithms used supplied training data for building library of TOI-s and to perform inversion and classification for the SLO test are described in Section 2.4. Using the inversion, clustering and classification procedures outlined above we produced a ranked anomaly list formatted as specified by the IDA[18].

6   COST ASSESSMENT

This work conducted under the SERDP#1572 project. There were some code development and adjustment during these classification studies, which are excluded from cost assessment. We did our best to track time and resources for each classification task. A summary of the time needed to classify each anomaly appears in Table 4. The quoted values are, of course, averages: some anomalies can be identified almost instantaneously, while others require much more time and effort.

Table 4: Cost model for advanced EMI model demonstration at SLO

Cost Category	Description	Cost
Pre-processing	Time required to analyze training data and check data quality, build the total NSMS library for TOI-s	60 sec/anomaly
Parameter extraction	Time required extract target feature parameters for test data	40 sec/anomaly
Classifier training	Time required to optimize classifier using the training data set.	40 sec/anomaly
Library matching technique	Time required for an expert: to visually inspect the inverted total NSMS and compare them to a library target's total NSMS; to make classification decision.	120 sec/anomaly
Classification and construction of a ranked anomaly list	Time required to classify anomalies in the test set and construct the ranked anomaly list	60 sec/anomaly
	Total	320 sec/anomaly

7   MANAGEMENT AND STAFFING

Figure 16 is the organization chart for the personnel involved in the demonstration. Their responsibilities are as follows:

1. Fridon Shubitidze – Principal Investigator. Developed and implemented most of the preprocessing and inversion routines used. Classified MetalMapper data and BUD data sets using library matching and a Gaussian mixture model.
2. Irma Shamatava – Sky Research Geophysicist. Participated in the inversion and classification of TEMTADS data.
3. David Karkashadze − A visiting professor at Dartmouth College. Classified TEMTADS data using library matching and semi-supervised parameter clustering.
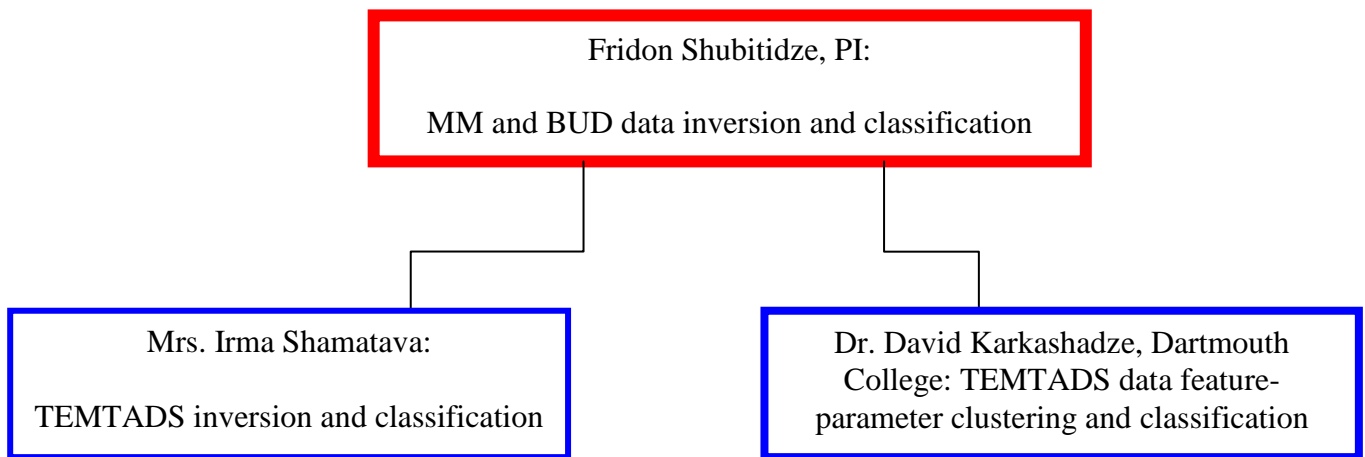
Figure 16: Project management hierarchy.

REFERENCES

[1]   H. Nelson*, et al.*, "ESTCP Pilot Program, Classification Approaches in Munitions Response," in *Environmental Security Technology Certification Program*, Arlington, VA, 2007.

[2]   ESTCP, "2010 ESTCP UXO Classification Study, Former Camp Butner, NC," presented at the Environmental Security Technology Certification Program Demonstration Plan, Arlington, VA, 2010.

[3]   ESTCP, "ESTCP Munitions Response, Live Site Demonstrations, former Camp Beale, CA, April 2011, Draft 4," June 2, 2011 2011.

[4]   ESTCP, "2009 ESTCP UXO Classification Study, Former Camp San Luis Obispo, CA," presented at the Environmental Security Technology Certification Program Demonstration Plan, Arlington, VA, 2009.

[5]   F. Shubitidze, "A complex approach to UXO discrimination: combining advanced EMI forward models and statistical signal processing," Sky Research Inc.2012.

[6]   I. Shamatava*, et al.*, "Live-site UXO classification studies using advanced EMI and statistical models," in *SPIE*, 2011.

[7]   I. Shamatava*, et al.*, "Applying the physically complete EMI models to the ESTCP Camp Sibert Pilot Study EM-63 data," presented at the Detection and Sensing of Mines, Explosive Objects, and Obscured Targets XIV, Orlando, FL, 2009.

[8]   I. Shamatava*, et al.*, "A physically complete model applied to BUD time-domain EMI data," in *SPIE*, 2009, p. 73030N.

[9]   I. Shamatava*, et al.*, "Physically complete models applied to BUD time-domain EMI data," presented at the Detection and Sensing of Mines, Explosive Objects, and Obscured Targets XIV, Orlando, FL, 2009.

[10] I. Shamatava*, et al.*, "SLO blind data set inversion and classification using physically complete models," in *SPIE*, 2010, p. 766404.

[11] M. Prouty, "Detection and Classification with the MetalMapper™ at Former Camp San Luis Obispo," presented at the ESTCP Project No. MM-0603, Geometrics, Inc, 2009.

[12] I. Shamatava*, et al.*, "Simple magnetic charge model for representation of emi responses from a buried UXO," in *DIPED*, 2004, pp. 155-159.

[13] F. Shubitidze*, et al.*, "Application of the normalized surface magnetic charge model to UXO discrimination in cases with overlapping signals," *Journal of Applied Geophysics,* vol. 61, pp. 292-303, 2007.

[14] F. Shubitidze*, et al.*, "A simple magnetic charge model for classification of multiple buried metallic objects in cases with overlapping signals," in *SAGEEP*, 2005.

[15] F. Shubitidze*, et al.*, "Combined differential evolution and surface magnetic charge model algorithm for discrimination of UXO from non-UXO items: simple and general inversions," in *SPIE*, 2005, p. 346.

[16] J. D. Jackson, *Classical Electrodynamics*, 3rd ed. New York: Wiley, 1999.

[17] F. Shubitidze, "Demonstration of Advanced EMI Models for Live-Site UXO Discrimination at Camp Butner, NC," 2012.

[18] S. Cazares and M. Tuley, "UXO Classification Study: Scoring Memorandum for the former Camp San Luis Obispo, CA," ed: Institute for Defense Analyses, 2009.

APPENDICES

7.1   Appendix A: Health and Safety Plan (HASP)

As this effort does not involve field data collection, no HASP is required.

7.2   Appendix B: Points of Contact

Points of contact (POCs) involved in the demonstration and their contact information are presented in Table 5.

Table 5: Points of Contact for the advanced EMI models' demonstration

POINT OF CONTACT Name	ORGANIZATION Name Address	Phone Fax E-mail	Role in Project
Dr. Fridon Shubitidze	Sky Research, Inc.	Tel: 603 643 2876 Fax: 603-643-5161 fridon.shubitidze@skyresearch.com	PI
Erik Russell	Sky Research, Inc. 3 Schoolhouse Ln, Etna, NH 03750, USA	Tel: 541-552-5197 Fax: 603-643-5161 Erik.Russell@skyresearch.com	Project Coordinator
Dr. Herb Nelson	ESTCP Program Office, ESTCP Office 901 North Stuart St, Suite 303 Arlington, VA 22203-1821	Tel: 571 372-6400 Herbert.Nelson@osd.mil	ESTCP Munitions Management Program Manager